Journal of Magnetic Resonance **137,** 265–271 (1999)
Article ID jmre.1998.1680, available online at http://www.idealibrary.com on IDEAL®

Current-Induced Magnetic Resonance Phase Imaging

J. Bodurka,*,† A. Jesmanowicz,* J. S. Hyde,* H. Xu,* L. Estkowski,* and S.-J. Li*,[1]

**Biophysics Research Institute, Medical College of Wisconsin, Milwaukee, Wisconsin 53226; and †Department of Biophysics, University School of Medical Sciences, Bydgoszcz 85-067, Poland*

Received August 5, 1998; revised November 3, 1998

Electric current-induced phase alternations have been imaged by fast magnetic resonance image (MRI) technology. We measured the magnetic resonance phase images induced by pulsed current stimulation from a phantom and detected its sensitivity. The pulsed current-induced phase image demonstrated the feasibility to detect phase changes of the proton magnetic resonance signal that could mimic neuronal firing. At the present experimental setting, a magnetic field strength change of 1.7 ± 0.3 nT can be detected. We also calculated the averaged value of the magnetic flux density B_T parallel to B_0 produced by electric current I inside the voxel as a function of the wire position. The results of the calculation were consistent with our observation that for the same experimental setting the current-induced phase change could vary with location of the wire inside the voxel. We discuss our findings in terms of possible direct MRI detection of neuronal activity.

Key Words: **electric current; magnetic field; MRI; phase imaging; neuronal activity.**

INTRODUCTION

Electric currents are used in numerous biomedical applications such as electrical impedance tomography, cardiac defibrillation, electrocautery, and physiotherapy (*1*). In particular magnetic resonance current-density imaging has been utilized to create images of electric current density in homogenous and heterogeneous media (*2, 3*). Recently, human brain mapping technology has been advanced based on integrated analysis of anatomical and functional measurement (*4, 5*). Magnetoencephalography and electroencephalography provide excellent temporal resolution of neuronal population dynamics as well as capabilities for source localization (*6, 7*). The recent development of functional magnetic resonance imaging (fMRI) techniques provides a unique method to map human brain function based on changes of blood flow and/or blood oxygenation level dependent (BOLD) contrast. In addition to high spatial resolution, fMRI permits detection of local changes in cerebral blood volume, flow, and oxygenation. These hemodynamic changes are attributed to neuronal activity (*8–10*). However, this is an indirect measurement of neuronal activity and has 2 to 5 s latency following neuronal stimulation onset. An ideal approach is to directly detect neuronal electric firing. The direct physical indication of local neuronal activity is the flow of ionic current across the neuron cell membrane, along the

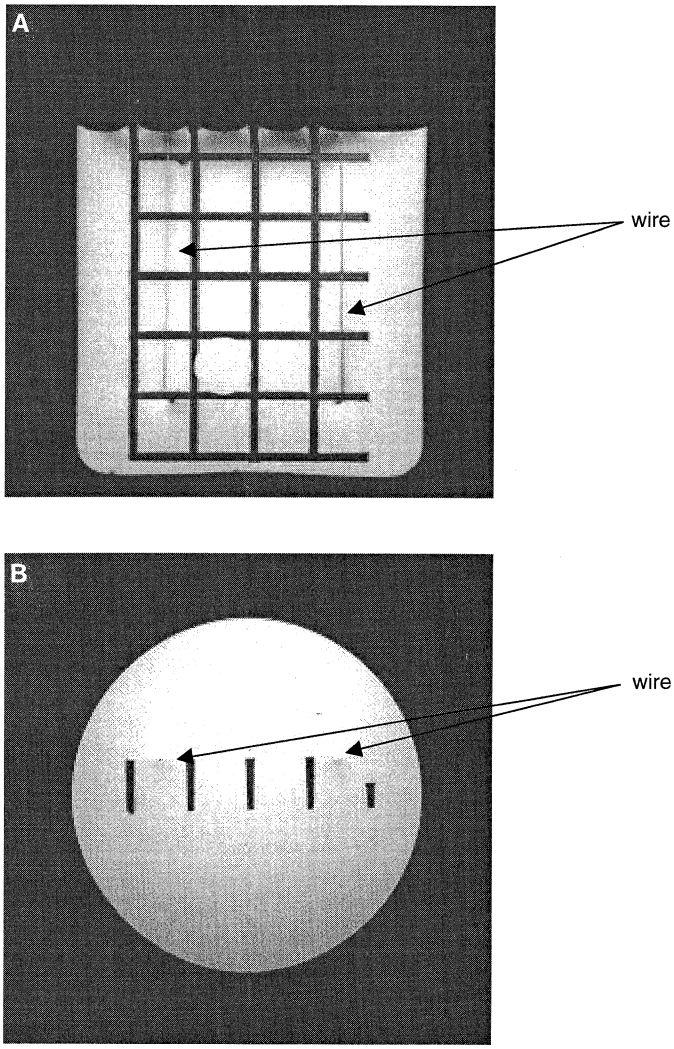

FIG. 1. (A) The axial image of the phantom. (B) A single coronal slice across the phantom used for fast imaging.

[1] To whom correspondence should be addressed at Biophysics Research Institute, Medical College of Wisconsin, 8701 Watertown Plank Road, Milwaukee, WI 53226. Fax: (414) 456-6512. E-mail: sjli@mcw.edu.

1090-7807/99 $30.00

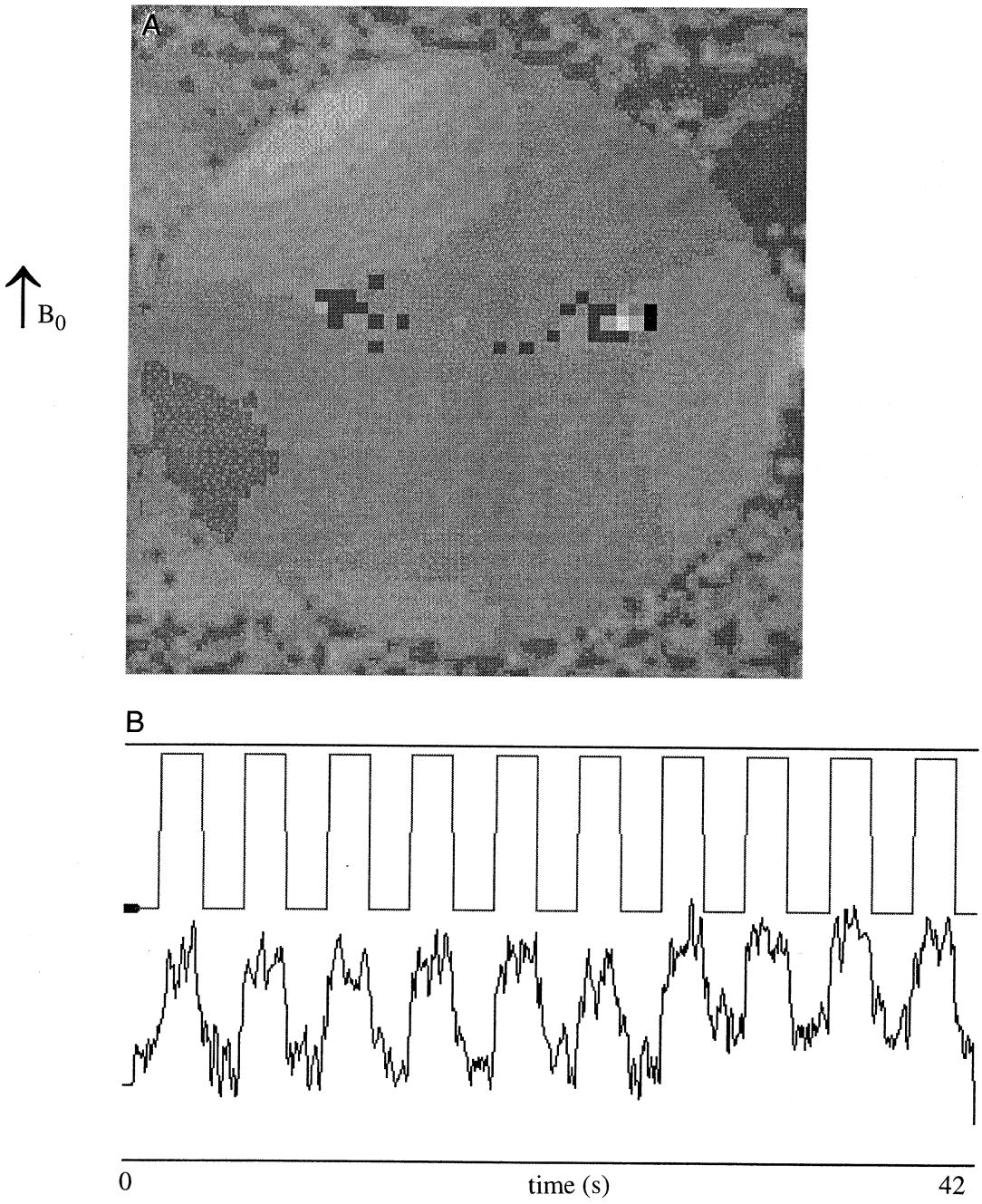

FIG. 2. The correlation map (A) and the time series (B) of the phase changes (together with the boxcar waveform) induced by a 70-μA current.

interior of the axon, and in the surrounding medium. This ionic current will produce another magnetic flux density (B_c), that, superimposed with B_0 field, will alter the phase of surrounding water protons. We hypothesize that electric current-induced phase alternations could be imaged by fast magnetic resonance imaging (MRI) technology. To demonstrate the feasibility of our hypothesis, we present the magnetic resonance phase images from a phantom induced by pulsed current stimulation and detect its sensitivity.

MATERIALS AND METHODS

A phase image phantom was constructed with an electrically insulated thin copper wire (60 μm diameter) formed into a 3-inch long and 2-inch wide rectangle that was supported by a plastic frame. The "anatomical" axial image of the phantom is shown in Fig. 1A. The plastic frame was immersed into a 500-ml water solution containing 0.75% NaCl, 5 mM $CuSO_4$. The orientation of the wire was perpendicular to the main

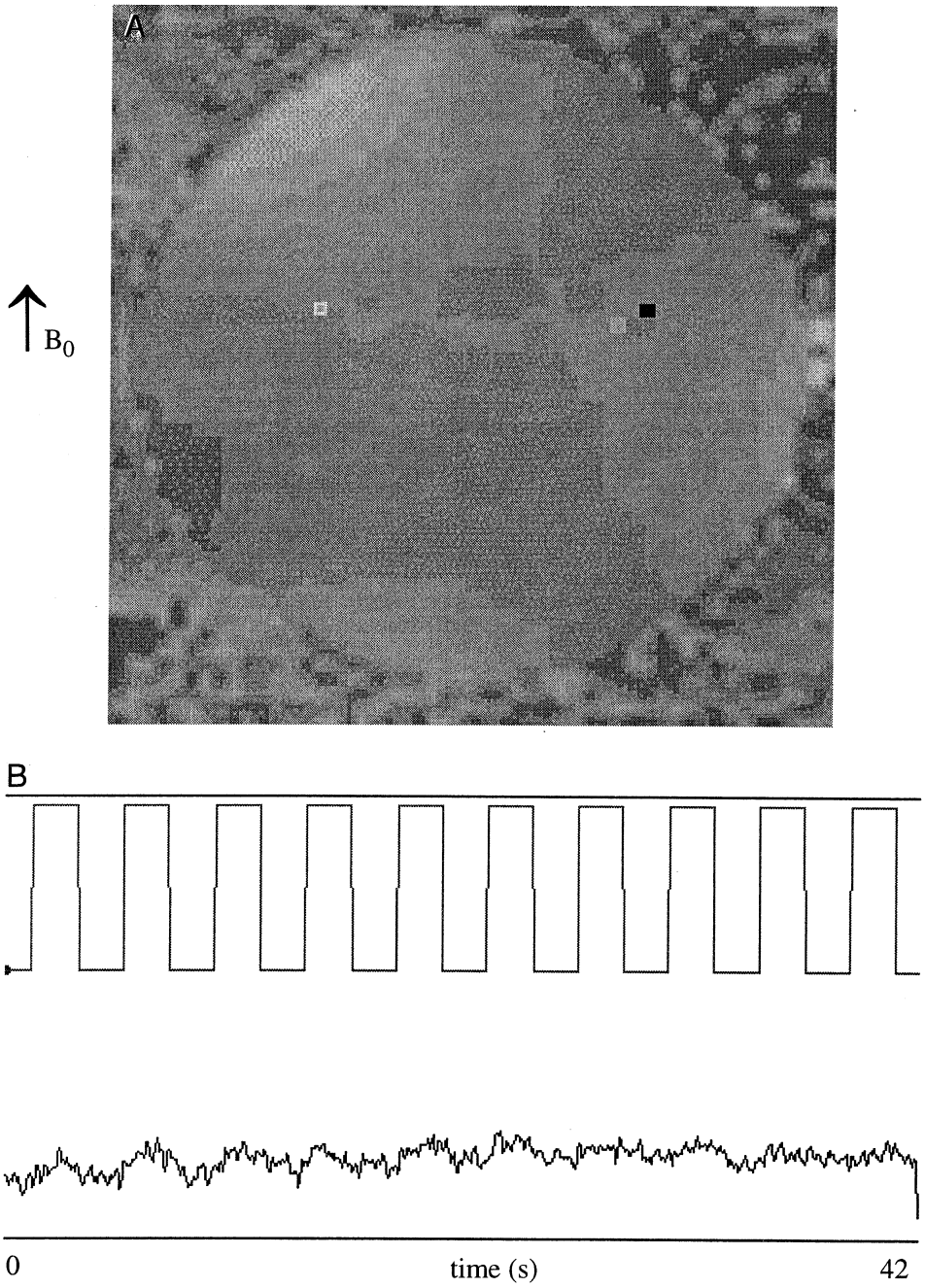

FIG. 3. The correlation map (A) and the time series (B) of the phase changes (together with the boxcar waveform) induced by a 10-μA current.

magnetic field B_0. A 10-k resistor was connected in series. A pulse generator (DG535, Stanford Research System, Inc, Sunnyvale, CA) was employed to provide a 0-, 10-, 20-, 30-, 50-, 70-, or 100-μA current with 2 s on and 2 s off cycle through the wire.

The experiment was performed on a Bruker Medspec scanner (3T/60 cm) with a homemade balanced torque three-axis local head gradient coil and endcapped bandpass birdcage RF head coil (*11, 12*). For fast imaging we used a single coronal slice across the phantom (Fig. 1B). Two wires were perpendicular to the main field B_0 and the current I passed through the parallel wires in the opposite direction. Localization of the measured slice was achieved with the fast gradient echo pulse sequence (TR/TE 200/10 ms, FOV 12 cm, matrix size 256 $\times$ 256). A gradient-recalled echo-planar imaging (EPI) sequence was used for fast imaging. The image parameters were TR 54 ms or 100 ms TE 27.2 ms, bandwidth $\pm$65.5 kHz, FOV 12 cm, image matrix 64 $\times$ 64, slice thickness 7 mm. The raw k-space

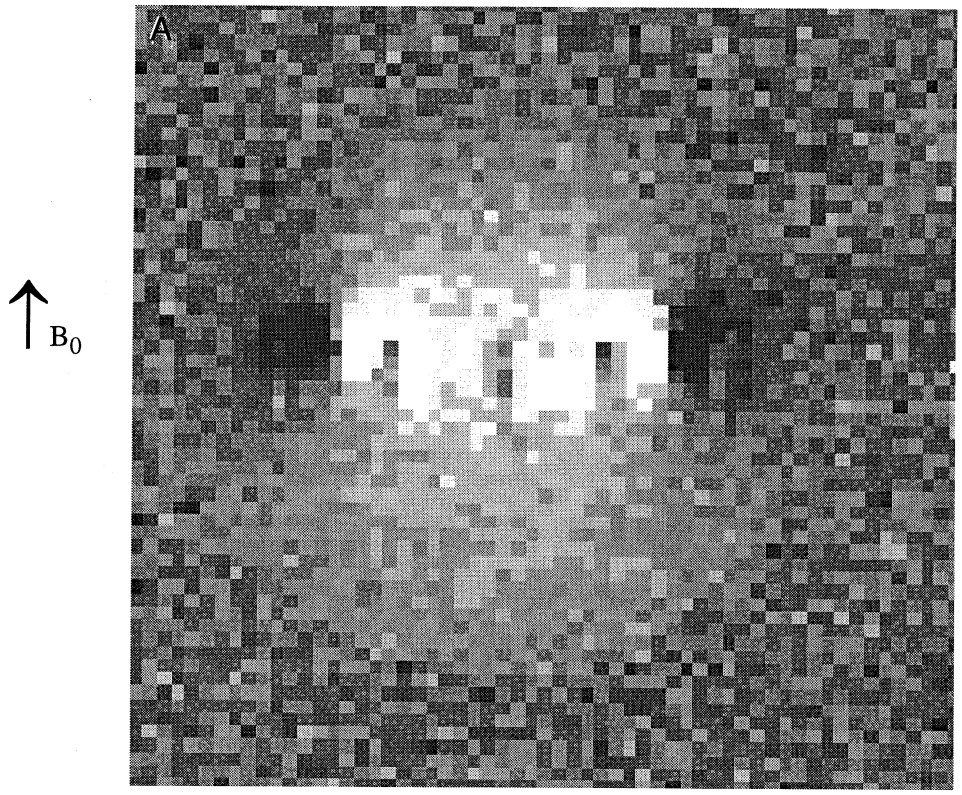

FIG. 4. The correlation image of the phase changes induced by a 70-μA current.

data sets were processed using self-correcting EPI reconstruction algorithm (*13*) and produced amplitude and phase images. The resulting dataset consisted of N phase or amplitude images acquired from the same coronal slice of the phantom at equally spaced time intervals. An "ideal" boxcar function with 2 s on and 2 s off cycle was used for cross-correlation (*14*). The amount of phase change ($\Delta\phi$) was obtained from phase images and its magnetic flux density change (ΔB) was calculated based on the echo time used and amount of phase change: $\Delta B = \Delta\phi/(\gamma \mathrm{TE})$.

RESULTS

We found that a time course of phase images has better sensitivity than a time course of amplitude images to detect current-induced magnetic field changes. In general the ability to observe a phase change in a magnetic resonance image depends on the signal-to-noise ratio (SNR) of the image (*3*). The phase noise standard deviation is approximately equal to 1/SNR. In our experiments, however, only contrast-to-noise is of interest because we are mainly focused on the current-induced relative phase changes. The standard deviation of phase noise in our time series was equal to 0.016 rad which corresponds to $\Delta B = 2.2$ nT. Figures 2 and 3 show the current-induced (70 and 10 μA, respectively) phase images (A) and time series of induced phase changes (B). Because the

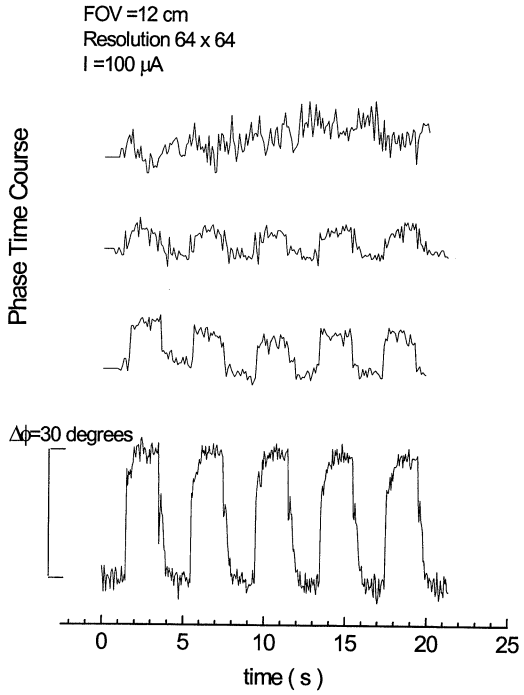

FIG. 5. The current-induced maximal positive phase change as a function of time obtained in four independent experiments with the same acquisition parameters TR/TE 54/27 ms, FOV = 12 cm, resolution 64 × 64, $I = 100$ μA.

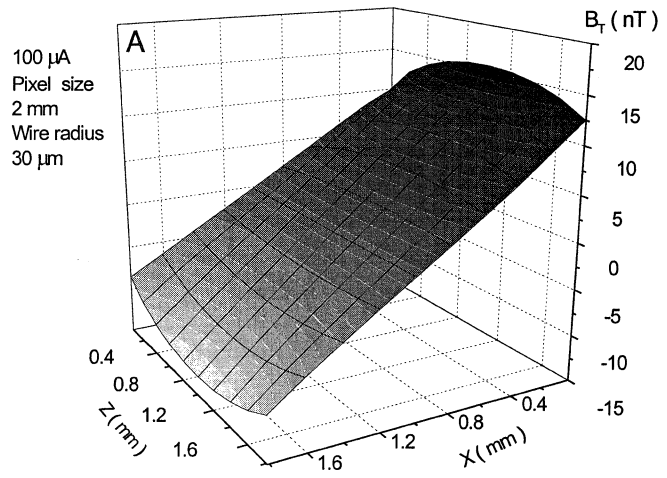

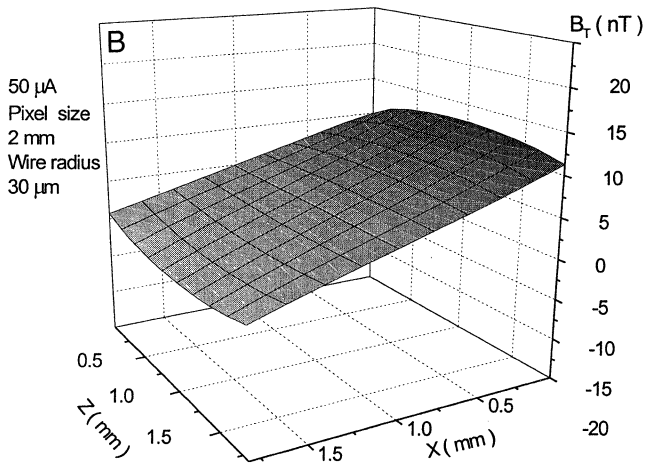

FIG. 6. The averaged B_T value of the Z component of B_c, parallel to B_0, produced by electric currents of 100 μA (A) and 50 μA (B) calculated as a function of wire position inside the single square pixel (pixel size 2 mm). The wire radius was 30 μm.

magnetic flux density induced by the electric currents (B_c) used in this study is much smaller than the external magnetic flux density (B_0), the most pronounced phase changes should be expected only in the direction parallel ($\Delta B = B_0 + B_c$) or antiparallel ($\Delta B = B_0 - B_c$) to B_0. Indeed the induced positive and negative phase changes occurred mainly in the left or right direction relative to the wire position corresponding to parallel and antiparallel components of the induced field (B_c) to B_0. To check that the current-induced phase changes were not EPI artifacts related to phase-encoding directions, we swapped the phase and the readout gradients. The observed phase changes were in the same positions (still parallel and antiparallel to B_0) but phase-encoded artifacts were rotated by 90°. It is interesting to note that the "on/off" and "off/on" current-induced phase changes are instantaneous, in contrast to the delayed BOLD signal-induced changes (*10*). The correlation image (Fig. 4) shows two pairs of black (decreased field) and white (increased field) regions located at each left/right side of the wires. Because the currents in the two wires flow in opposite directions, the white regions are inside and the black regions are outside the wires. Figure 3 demonstrates the sensitivity of a phase image, for current as low as 10 μA the same features were observed. We have calculated the induced change of magnetic field to be 1.7 ± 0.3 nT.

During several independent experiments we observed that for the same experimental setting (slice position and thickness, resolution, TR/TE, and current amplitude) the maximal induced phase change varied (Fig. 5). However, the wire positions within a single voxel in each experiment were not the same due to slightly different phantom position inside the gradient coil. Ideally, if the wire is located in the center of the voxel, the observed phase change from this voxel should be

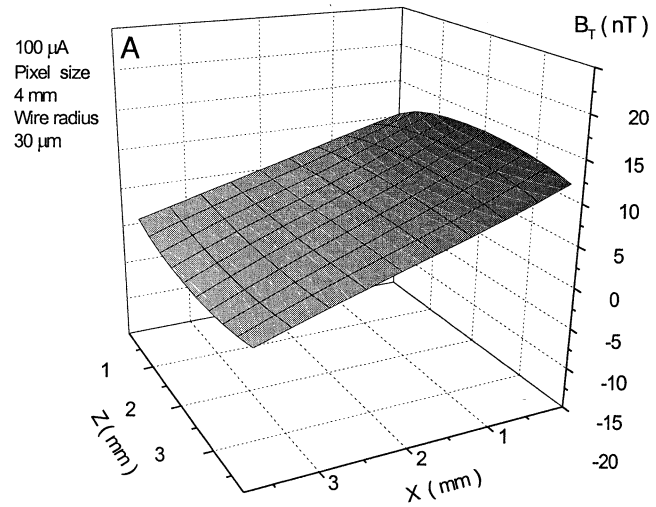

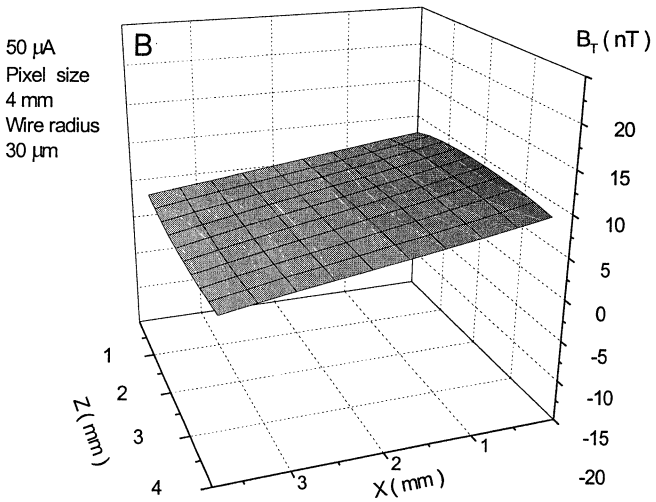

FIG. 7. The averaged B_T value of the Z component of B_c, parallel to B_0, produced by electric currents of 100 μA (A) and 50 μA (B) calculated as a function of wire position inside the single square pixel (pixel size 4 mm). The wire radius was 30 μm.

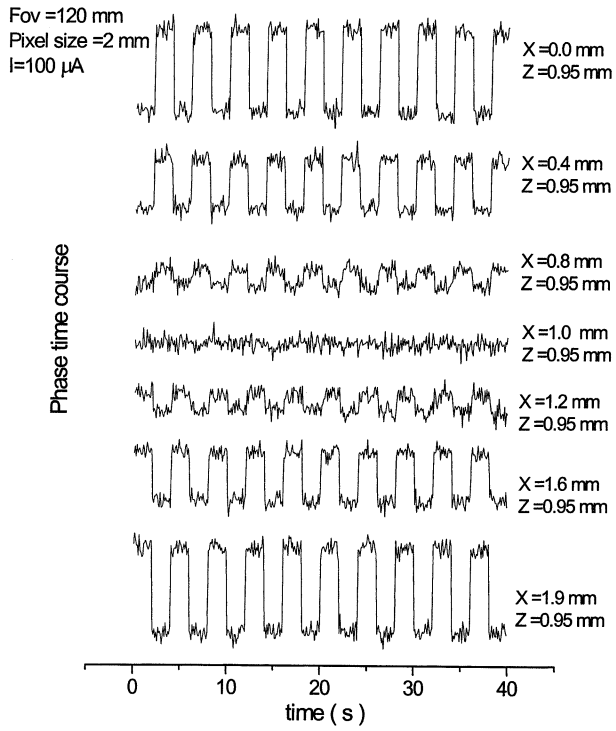

FIG. 8. The simulated phase changes with gaussian noise as a function of time corresponding to different wire positions inside the voxel.

zero due to inherent cancellation of the parallel and antiparallel (to B_0) field components. The opposite phase change can be observed in the adjacent left/right voxels; however, the amplitude of change decreases with the distance from the wire. Therefore we calculated the average value B_T, of Z component of B_c parallel to B_0 produced by the electric current inside the voxel as a function of the wire position. We have assumed that the net phase change in a voxel can be evaluated from $\Delta\phi/\mathrm{TE} \cong (\gamma B_T)$. For simplicity we assumed that our wire is infinitely long. The magnetic flux density components B_{cX} and B_{cZ} produced in the ZX plane by the wire oriented parallel to the Y axis are

$$B_{cX} = -\frac{\mu_0}{4\pi} 2I \frac{z}{x^2 + z^2} \qquad B_{cZ} = \frac{\mu_0}{4\pi} 2I \frac{x}{x^2 + z^2}, \quad [1]$$

where $x^2 + z^2$ is the distance from the wire and I is the current intensity. So the average magnetic flux density parallel to B_0 produced by electric current inside the voxel is

$$B_T = \frac{1}{L_X L_Y L_Z} \int_V B_{cZ}(x, z)dV = \frac{1}{L_X L_Z} \int_S B_{cZ}(x, z)dS, \quad [2]$$

where $V = L_X L_Y L_Z$ is the voxel volume and $S = L_X L_Z$ is the pixel area.

The results of numerical calculation of Eq. [2] for two square pixel ($L_X = L_Z$) sizes, 2 and 4 mm, and two different currents, 100 and 50 μA, and wire diameter 60 μm are shown in Figs. 6A and 6B and 7A and 7B, respectively. As expected, when the wire is located in the vicinity of the voxel center the current-induced magnetic field is close to zero and the current-induced phase changes are minimal. When the wire position is moved towards the pixel X edges, the B_T value increases and reaches a maximum for $z = L_Z/2$ and $x = a_0$ or $x = (L_X - a_0)$, where a_0 is the wire radius. Figure 8 shows the simulated phase changes as a function of time corresponding to different wire positions inside the voxel. The results of the calculation are consistent with our observation (Fig. 5) that for the same experimental setting the current-induced phase change could vary with location of the wire inside the voxel.

DISCUSSION

The current-induced phase images demonstrated the feasibility of detecting phase changes of the proton magnetic resonance signal that could mimic neuronal firing. Changes of the magnetic field strength 1.7 ± 0.3 nT were detectable. Roth and Wiskwo have calculated the magnetic field due to an action potential propagating down a crayfish axon embedded in an infinite homogenous conducting medium (*15, 16*). The maximal field strength of about 1 nT was calculated for the distance of 0.12 mm from the axon. This value corresponds to ionic current flow along the interior of the axon of the order of microamperes. However, the ionic current in a single neuron is of the order of picoamperes and results in a magnetic field strength of the order of 10^{-15} T (*16*). For comparison, the field strength from lung particles is $\approx 10^{-9}$ T, from magnetocardiogram is $\approx 10^{-10}$ T, from the brain 10^{-12} T for spontaneous (α wave) activity, and 10^{-13} T for evoked response (*17, 18*). These magnetic field changes are far beyond MRI detection capabilities. The magnetic field strength produced by a single neuron is obviously too small to be measured by MRI; however, if, for example, 10^6 parallel-oriented neurons act together then the resulting magnetic field could be detectable. We believe that future work will result in the direct *in vivo* detection of electric neuronal activity.

CONCLUSION

The current-induced phase images demonstrated the feasibility of detecting phase changes of the proton magnetic resonance signal that could mimic neuronal firing. The magnetic field changes of 1.7 ± 0.3 nT were detectable due to electric current as small as 10 μA. The phase changes induced by the pulse electric current depend on the wire position inside the voxel. We calculated the average value of the Z component of B_c parallel to B_0 produced by electric current I inside the voxel (B_T) as a function of the wire position. The results of the calculation explain our finding that for the same experimental

setting the current-induced phase change could vary with location of the wire inside the voxel.

ACKNOWLEDGMENTS

This work was supported in part by Grant DA10214 from the National Institute on Drug Abuse. The authors thank Ms. Hollis Brunner for editorial assistance.

REFERENCES

1. C. J. Kotre, Electrical impedance tomography, *Br. J. Radiol.* **70,** 200–205 (1997).
2. G. C. Scott, M. L. G. Joy, R. L. Armstrong, and R. M. Henkelman, RF current density imaging in homogeneous media, *Magn. Reson. Med.* **28,** 186–201 (1992).
3. G. C. Scott, M. L. G. Joy, R. L. Armstrong, and R. M. Henkelman, Sensitivity of magnetic resonance current density imaging, *J. Magn. Reson.* **97,** 235–254 (1992).
4. J. S. George, C. J. Aine, J. C. Mosher, D. M. Schmidt, D. M. Ranken, H. A. Schlitt, C. C. Wood, J. D. Lewine, J. A. Sanders, and J. W. Belliveau, Mapping function in the human brain with magnetoencephalography, anatomical magnetic resonance imaging, and functional magnetic resonance imaginig, *J. Clin. Neurophysiol.* **12,** 406–431 (1995).
5. A. Jesmanowicz, J. Myklebust, J. Blimke, and J. S. Hyde, Simultaneously EEG correlation with resting-state vector time courses in fast EPI, *in* "Proceedings: International Society for Magnetic Resonance in Medicine, 6th Annual Meeting, Sydney," p. 105, International Society for Magnetic Resonance in Medicine, Berkeley, CA (1998).
6. J. D. Lewine, Magnetoencephalography and magnetic source imaging, *in* "Functional Brain Imaging" (W. W. Orrison, J. D. Lewine, J. A. Sander, and M. F. Hartshorne, Eds.), pp. 369–417, Mosby, St. Louis (1995).
7. J. D. Lewine and W. W. Orrison, Clinical electoencephalography and event-related potentials, *in* "Functional Brain Imaging" (W. W. Orrison, J. D. Lewine, J. A. Sander, and M. F. Hartshorne, Eds.), pp. 327–368, Mosby, St. Louis (1995).
8. S. Ogawa, D. W. Tank, and R. Menon, Intrinsic signal changes accompanying sensor stimulation: Functional brain mapping using MRI, *Proc. Natl. Acad. Sci. USA* **89,** 5951–5955 (1992).
9. P. A. Bandettini, E. C. Wong, R. S. Hinks, R. S. Tikofsky, and J. S. Hyde, Time course EPI of human brain function during task activation, *Magn. Reson. Med.* **25,** 390–397 (1992).
10. P. A. Bandettini, E. C. Wong, J. R. Binder, S. M. Rao, A. Jesmanowicz, E. A. Aaron, T. F. Lowry, H. V. Forster, R. S. Hinks, and J. S. Hyde, Functional MR Imaging using BOLD approach, *in* "Diffusion and Perfusion Magnetic Resonance Imaging" (D. L. Bihan, Ed.), pp. 335–349, Raven Press, New York (1995).
11. E. C. Wong, P. A. Bandettini, and J. S. Hyde, EPI imaging of the human brain using a three axis local gradient coil, *in* "Proceedings: Society of Magnetic Resonance in Medicine, 11th Annual Meeting, Berlin," p. 105, International Society for Magnetic Resonance in Medicine, Berkeley, CA (1992).
12. E. C. Wong, G. Tan, and J. S. Hyde, A quadrature transmit-receive endcapped birdcage coil for imaging of the human head at 125 MHz, *in* "Proceedings: Society of Magnetic Resonance in Medicine, 12th Annual Meeting, New York," p. 1344, International Society for Magnetic Resonance in Medicine, Berkeley, CA (1993).
13. A. Jesmanowicz, E. C. Wong and J. S. Hyde, Self-correcting EPI reconstruction algorithm, *in* "Proceedings: Society of Magnetic Resonance in Medicine, 3rd Scientific Meeting and Exhibition, Nice," p. 619, International Society for Magnetic Resonance in Medicine, Berkeley, CA (1995).
14. P. A. Bandettini, A. Jesmanowicz, E. C. Wong, and J. S. Hyde, Processing strategies for time-course data sets in functional MRI of the human brain, *Magn. Reson. Med.* **30,** 161–173 (1993).
15. B. J. Roth and J. P. Wikswo, The magnetic field of a single axon: A comparison of theory and experiment, *Biophys. J.* **48,** 93–109 (1985).
16. R. K. Hobbie, "Intermediate Physics for Medicine and Biology," Springer-Verlag, New York (1997).
17. D. Cohen and I. Nemoto, Ferromagnetic particles in the lung. Part I. The magnetizing process. *IEEE Trans. Biomed. Eng.* **BME-31,** 261–273 (1984).
18. G. Stroink, M. J. R. Lamothe, and M. J. Gardner, Magnetocardiographic and electrocardiographic mapping studies, *in* "SQUID Sensors: Fundamentals, Fabrications and Applications" (H. Weinstock, Ed.), pp. 121–134, NATO ASI Series, Kluwer Academic, The Netherlands (1993).